Complex ceramic architectures by directed assembly of 'responsive' particles

Esther García-Tuñón [a,*], Gil C. Machado [a], Marc Schneider [b], Suelen Barg [c], Robert V. Bell [d], Eduardo Saiz [a]

[a] Department of Materials, Imperial College London, South Kensington, London, SW7 2BP, UK
[b] MT.Derm GmbH, Blohmstraße 37-61, Berlin, 12307, Germany
[c] School of Materials, Manchester University, Oxford Road, Manchester, M13 9PL, UK
[d] Department of Chemistry, University of Warwick, Coventry, CV4 7AL, UK

1. Introduction

Based on lessons from nature, scientists have been designing materials that respond to stimulus in the same way that living systems respond to subtle changes on their environment [1]. Applications of synthetic 'responsive' polymers in drug delivery, tissue engineering or cell mediation have been studied extensively and numerous papers and patents evidence a rapid growing field [1,2]. Responsive polymers are characterized by a reversible response to external stimuli; they are capable of changing their configuration or properties under a change of pH, stress, light or temperature [3–5]. Recent works on surface engineering describe responsive surfaces that, for example, switch from super hydrophobic to superhydrophilic in response to light, temperature, pH or stress [1,3,6]. However, these advances have not been applied before in wet processing of ceramics.

On the other hand, the design and manufacturing of cellular structures is a widely investigated area in materials science. Thanks to their unique combination of properties and functionalities (for example they can be light and strong), porous materials are used in many applications for engineering and medicine. From catalysis supports, filters, separation membranes, thermal insulators, reinforcement of composites to scaffolds for bone replacement [7–9]. However, shaping bulk materials in porous hierarchical structures with practical dimensions, controlled morphological features at multiple scale lengths and multifunctional properties, is still a challenge in materials science. Freeze casting, foaming, emulsion and sacrificial templating are some of the techniques currently available to create cellular materials. Freeze casting uses the complex structure of ice to create materials that exhibit bio-inspired hierarchical structures and promising properties [10]. Foaming of colloidal particles functionalized with short chain amphiphile molecules leads to very ultra-stable wet ceramic foams, that can be consolidated into highly porous foams [11]. Sacrificial templating uses natural or synthetic hard templates (for example polymeric foams, wood or coral) and impregnation of colloidal suspensions to create ceramic foams with the same structure as the original template [9]. Emulsion templating is another path used to fabricate cellular ceramics, metals and polymers [12–20]. Although particle stabilised emulsions are known for more than a century [21], many authors have

* Corresponding author.
E-mail address: egarciat@imperial.ac.uk (E. García-Tuñón).

delved into their understanding and application to build cellular materials in recent studies [13,15,22,23]. The oil droplets act as a temporary template and determine the morphological features in the final porous structures.

Despite the availability of these wet-processing techniques, there are still some challenges to overcome. For example, these approaches are often limited to the fabrication of monoliths with very simple shapes, like cubes or cylinders. Another disadvantage is their limited flexibility. Some of these techniques are specifically optimized for certain materials and additives, also making difficult the scaling up in a manufacturing process. It is necessary to formulate and integrate new basic science into practical manufacturing techniques to overcome some of the current processing limitations.

In this work we aim to integrate a bottom-up particle assembly approach inspired by natural processes – such as the directed assembly of DNA molecules and other proteins in living organisms – into traditional ("top-down") processing technologies. This combination enables building hierarchical ceramic structures with complex shapes at the macro scale [12]. The objective is to develop a novel manufacturing route based on the design of 'responsive' particles that 'self-assemble' on-demand into hierarchical architectures. We use a responsive polymer – namely branched copolymer surfactant (BCS) – to functionalise the surface of alumina particles and make them react to pH changes [12,24]. Here we delve into the basic science involved in this processing approach: from the basic mechanisms involved in surface functionalization, interface stabilisation and emulsification and their effects in the final microstructures, to the effects of different parameters in aggregation kinetics and network stiffness. We describe how to create highly dense and porous ceramic components with a wide range of morphological features (total porosities varying between 50 and 83% with open porosities between 55 and 70% and pore size from 30 to <4 μm) and provide additional results of their mechanical performance.

2. Experimental section

2.1. Particle functionalisation

BCS with a composition of $PEGMA_5/MAA_{95}$-$EGDMA_{10}$-DDT_{10} was synthesized following the protocol described in Refs. [24,25]. BCS solutions with compositions between 0.5 and 5 wt/vol% were prepared in distilled water at pH 8 (adjusted with NaOH). Alumina powders (Al_2O_3, Baikalox B-series SMA6, D_{50} = 0.3 μm, Baikowski, France) were sieved through 100 μm mesh to break down aggregates. Alumina suspensions (from 7 up to 43 vol%) were prepared by mixing the powders with BCS stock solutions and ball milling for at least 24 h. The suspensions were subsequently conditioned with 2.5 wt% of 1-octanol and stirring under a light vacuum.

2.2. Particle-BCS interactions

BCS functionalised-ceramic suspensions with 10 vol% of particles and increasing concentrations of BCS (from 0.25 to 5 wt/vol%) were prepared and analysed by dynamic light scattering (DLS) to measure the effective average particle size. The results were compared with the real average particle size (0.3 μm as given by the supplier) and also with the particle size distribution of alumina suspensions stabilised with an electro steric dispersant commonly used in ceramic processing, Dolapix CA (Zschimmer & Schwarz GmbH & Co). Additionally, to determine the BCS adsorption isotherm, the equilibrated alumina/BCS suspensions were subjected to centrifugation to sediment the particles. By quantifying the amount of sulphur in the supernatants (coming from the DDT chain ends) using inductive coupled spectroscopy (ICP), we could quantify the amount of BCS free molecules in the solution and determine the degree of adsorption of BCS onto the particles. Sulphur standard solutions (with concentrations between 0 and 100 ppm) were measured prior the analysis of BCS pattern solutions and supernatants. By measuring the sulphur contents of BCS solutions with concentrations ranging from 0 to 5 wt/vol% BCS, we obtained a calibration fitting to then determine the free BCS amounts in the supernatants.

2.3. Emulsification

Ceramic suspensions with solid loads between 7 and 43 vol% were emulsified with 50 vol% of decane, at stirring speeds ranging from 2000 to 24,000 rpm, by using either an IKA stirrer or IKA Ultraturrax homogenizer.

2.4. Interfacial energy measurements (IFT)

The interfacial (oil/continuous phase) energy of the emulsions was measured using the pendant drop method in a Dataphysics, Contact Angle System OCA (software SCA 20). First, the IFT of oil/BCS solutions (with increasing BCS concentrations, from 0.5 to 5 wt/vol%) were measured from a drop of BCS solution (volumes between 5 and 20 μL) inside an optically clear glass cuvette containing decane. Afterwards, droplets of alumina suspensions containing the same BCS concentrations and fixed solid loading (17 vol%) were also measured using the same method. Additionally, we evaluated the effect of the solid loading on the IFT for a fixed BCS concentration (1 wt/vol%) and increasing particle content.

A fluorescent molecule, Rhodamine, was incorporated into the branched BCS architecture in order to look at the segregation of polymer at the oil/water and oil/continuous phase (for the suspensions) interfaces. Images of emulsions and emulsified suspensions containing rhodamine modified BCS were taken with a Axio Scope.A1 ZEISS optical microscope, using an immersion 100× ocular (N-Achroplan 100×/1.25 Oil iris WD0.29M27), fluorescence free immersion oil and rhodamine fluorescence filter (FL Filter Set 43 CY 3 Shift free).

2.5. Assembly

We use a pH trigger, glucono-δ-lactone (GδL, ≥99%, Sigma Aldrich) to homogeneously drop the pH and control the assembly of particles in alumina suspensions and emulsions. GδL lowers the pH in a homogeneous two-step process, first dissolution and subsequent hydrolysis of the GδL to gluconic acid. Amounts of GδL ranging from 0.5 to 12 wt/vol% were added to drop the pH below the pK_a (6.46 [25]) of BCS and subsequently trigger the establishment of multiple inter- and intra- hydrogen bonds between the BCS molecules. For the production of dense components, concentrated alumina suspensions (43 vol%) were mixed with GδL, poured into the moulds and left until aggregation is completed inside a vacuum cast device (up to 90 min). In the case of porous materials, GδL was added to the emulsified suspensions by gently shaking the vials. The emulsions were then poured into the moulds and left setting at room temperature for at least 24 h before drying in a convective oven at 37 °C.

2.6. Rheology

Viscosity and viscoelasticity measurements were performed using a Discovery Hybrid Rheometer HR1 (TA Instruments). Viscosity measurements of alumina suspensions and emulsions were done with a conical (ø 60 mm) geometry and a solvent trap cover under steady sensing. Viscoelastic fingerprints and assembly processes were measured with a parallel plate (ø 40 mm) and solvent

trap cover. The aggregation process could be monitored from the change in the magnitude of the viscoelastic properties (G′, G″) over time (time sweep). The values of the storage modulus, G′, provided a measure of the strength of the particle network. Samples were prepared by mixing 2 mL of the suspensions and emulsions with amounts of GδL between 0.5 and 12 wt/vol%. After gently mixing for ~30 s, the samples were transferred to the rheometer. A conditioning step for 10 s was set prior running the time sweep. A time sweep at fixed frequency ($\omega = 1$ Hz) and displacement ($\theta = 5 \times 10^{-5}$ rad) was applied to follow the kinetics of the assembly for different suspensions and emulsions. The solvent trap cover prevented water evaporation, while axial force control allowed identifying changes in volume as well as automatically adjusting the gap. Viscoelastic fingerprints and linear viscosity regions (LVR) were evaluated with stress-controlled amplitude sweeps at a fixed frequency of 1 Hz.

2.7. Preparation of ceramic structures

High-density alumina components were prepared by triggering the assembly of alumina suspensions (43 vol% solids and 1–2 wt/vol% BCS), by adding amounts of GδL between 0.5 and 2 wt/vol%. Several drying conditions were tested: temperatures between 20 and 50 °C under forced convection, room temperature in air, as well as under vacuum at room temperature. High-density parts were achieved with a three-step drying process. First, after triggering the directed assembly the alumina suspensions were poured into moulds under vacuum (0.6 bar) until aggregation was complete (for ~90 min), thus encouraging the release of trapped air in the sample. The second drying step took place at room temperature in a desiccator for 48 h. After 24 h in the desiccator the samples could be easily handled and demoulded. After another 24 h, samples were ready for the final drying stage in an oven with forced convection at 40 °C for 24 h.

Alumina foams with a wide range of microstructures were prepared from emulsified suspensions (7–43 vol% solid loading in the continuous phase, and 50 vol% decane). GδL amounts between 1 and 10 wt/vol% (related to the continuous phase) were added to the emulsified suspensions before pouring them into moulds. Samples were left inside a desiccator at room temperature until they could be de-moulded and handled and subsequently dried in a convective oven at 40 °C. For samples with low solid loading (7–15 vol% in the continuous phase) drying at room temperature in air took place for up to three weeks before sintering. Both, highly dense and porous alumina materials, were sintered in a chamber furnace with a heating rate of 1 °C min^{-1} up to 500 °C; held for 2 h while the burning out of BCS takes place; afterwards the temperature was raised at 5 °C min^{-1} up to 1550 °C and then held for 1 h before cooling down to room temperature.

2.8. Characterization

Density and porosity were determined by the Archimedes method. The microstructure and morphological features of the materials were analysed in a Field Emission Scanning Electron Microscope (Gemini 1525 FEGSEM). Thermal etching on dense samples was carried at 1450 °C in air for 1 h after polishing with diamond particles of 1 μm size. Grain size for dense components and pore sizes and distributions for porous materials were quantified from FESEM images using the image analysis software ImageJ and Linear Intercept – Lince (TU Darmstadt) respectively.

Bending strengths and fracture toughness of highly dense alumina pieces were measured following the standards ASTM C1161-02c and ASTM C1421-10 respectively. Bars were cut, grinded and chamfered at 45° according to the standards. For the fracture toughness measurements, bars were notched in a two-step process: first with a 500 μm thick diamond blade, and then sharpening with a razor blade and the aid of 1 μm polishing suspensions. The pre-crack was sharpened until its length was 30% of the sample height.

The compressive strength of alumina foams was measured in a universal mechanical testing machine (model Z010, Zwick Roell, Germany), following the ASTM C133-94 standard with crosshead speeds ranging between 0.5–2 mm min^{-1}. For each material, 10–20 specimens measuring $5 \times 5 \times 5$ mm^3 were cut from a ceramic part with a diamond disk and grinded to ensure parallel surfaces. In order to homogeneously distribute the load during the compression tests, a stainless steel semi sphere was placed at the top of the samples. Bars were cut to measure their flexural strengths in three and four point bending (with a span at least 10 times the lateral size of the beams) at a constant crosshead speed of 1.3 mm/s.

3. Results and discussion

BCS (Fig. 1) is an amphiphilic pH-responsive branched copolymer composed of two main domains: poly (methacrylic acid) (PMAA) and polyethylene glycol (PEG) – which are crosslinked with

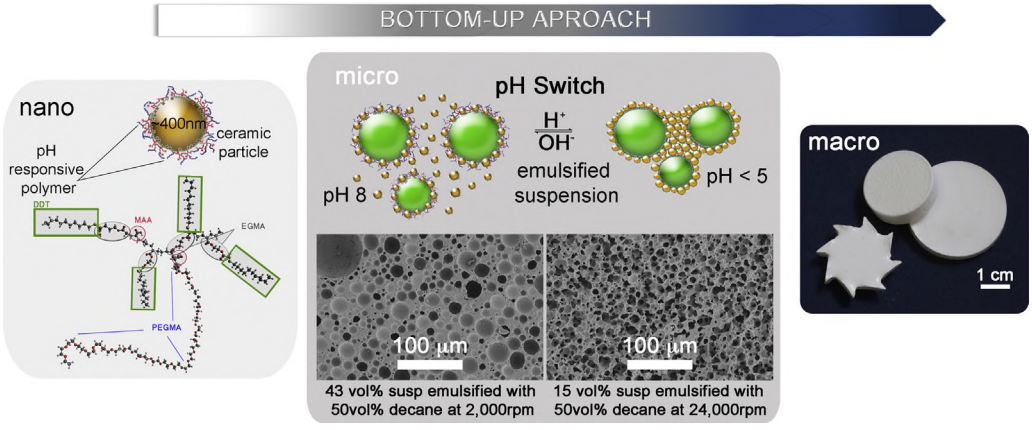

Fig. 1. Scheme showing the bottom-up approach to make porous complex ceramic structures. Bottom-At the nanometre scale, a simplification of the BCS branched architecture shows the multifunctional nature of this responsive polymer. PEGMA and PMAA branches are cross-linked by EGMA and multiple DDT chain ends provide hydrophobic anchoring points. BCS molecules adsorb onto the ceramic particles and provide stabilisation in water at pH values above pK_a for BCS. Middle-At the micrometre scale, the emulsification of BCS-stabilised alumina suspensions provides a delicate control of the morphological features. Top-At the macro scale, we can fabricate alumina components with intricate shapes and densities ranging from high (~99% of theoretical value for dense alumina) when working directly with BCS stabilised suspensions, to very low (up to 83% total porosity) when using emulsified suspensions.

ethylene glycol dimethacrylate (EGDMA) to provide a branched architecture [26,27]. Each of the polymer chain ends contains 1-dodecanethiol (DDT), which offer multiple hydrophobic anchoring groups. The composition and architecture of BCS provide multiple functional groups that enable the adsorption of BCS molecules onto the surfaces of alumina particles [12]. This surface functionalization simultaneously provides electro steric stabilisation and makes the particles responsive to pH. The interactions between the main domains (PEG and PMAA) on BCS at different pH values (above and below the pK_a of the BCS, 6.46 [25]) are responsible for the assembly of the particles. At pH values above the pK_a of BCS, all the carboxylic functionalities in PMAA groups are ionized providing electrostatic repulsions. When the pH drops below the pK_a, their protonation leads to the establishment of multiple non-covalent interactions by hydrogen bonding. In this way, a pH switch directs a controlled and reversible assembly of the particles below the pK_a of BCS. The aggregation of concentrated alumina suspensions leads to highly dense ceramic components with complex shapes (Fig. 1). The emulsification of these suspensions with decane results in emulsified suspensions with different properties (stability, rheology, droplet size and distribution) that lead to cellular ceramics with a wide range of microstructures (Fig. 1).

3.1. *Surface functionalization*

Surface functionalization takes place at pH ≤8 (using BCS stock solutions, see Section 2) when the MAA functionalities in BCS are in their anionic form and the alumina surfaces are slightly positively charged (to avoid the isoelectric point, IEP, at pH ≈ 9). Dynamic light scattering (DLS) and inductive coupled spectroscopy (ICP) provided an insight into BCS-particle interactions. DLS results showed that at low BCS concentrations (0–0.5 wt/vol%) the alumina particles were not completely stable and formed aggregates (Fig. 2a). Higher BCS concentrations (1–5 wt/vol%) provide stable suspensions, but amounts above 2 wt/vol% resulted in an increase of the average particle size probably due to the formation of BCS multilayers on the surface (Fig. 2a). BCS also showed better stabilisation capabilities than surfactants commonly used in ceramic processing, for example Dolapix (Fig. 2b). The average particle size of alumina stabilised with BCS matches the information provided by the supplier (D_{50} ~ 0.3 μm). However when using Dolapix with the same concentration the size distribution shows two broad peaks indicating that particles were forming aggregates (Fig. 2b).

ICP results show that the amount of BCS molecules adsorbed on the surfaces rapidly increases with increasing BCS amounts (Fig. 2c). When plotting the adsorption data against the BCS equilibrium concentration (Fig. 2d), the fitting to a Langmuir adsorption isotherm gives an adsorption constant (k) of 0.004 mL/mg and a maximum coverage (Γmax) of 47 mg/m^2 (Fig. 2d). Taking into account the molecular weight of the polymer (Mw = 28,163 g/mol [25]) this corresponds to ~1 molecule per nm^2, which is much smaller than the equivalent molecular diameter (~40 nm). These analyses are in good agreement with the particle size studies and suggest multilayer coverage on the particle surface. This precludes the interpretation using the Langmuir adsorption isotherm (Fig. 2d) [28], but we do not have enough experimental data to provide a reliable fitting to more complex models.

DLS and ICP results prove that at pH above its pK_a, BCS is a good dispersant of ceramic particles. BCS, an amphiphile with multifunctional-branched architecture, stabilises alumina particles in water, interacting with their surfaces and providing steric and electrostatic repulsion between them. This allows us to obtain high-solid loading and stable alumina suspensions up to 43 vol%. Attachment and functionalization take place through the following possible mechanisms: 1) electrostatic interactions between the carboxylic anions in the MAA residues with the positively charged

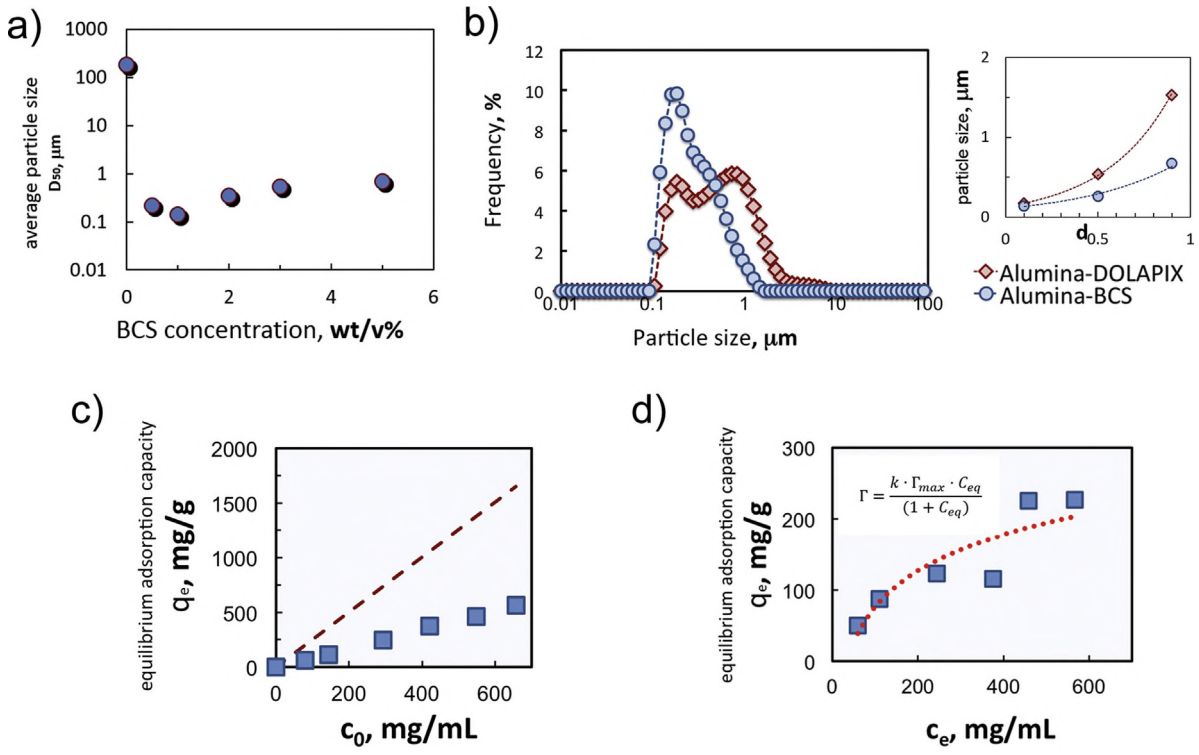

Fig. 2. Surface functionalization: BCS particle stabilisation (a, b) and adsorption isotherm (c, d). (a) Graph showing the average particle size of alumina powders functionalised with increasing amounts of BCS. Amounts <1 wt/vol% do not provide enough stabilisation; increasing BCS at concentrations above 2 wt/vol% multilayer adsorption leads to an increase in particle size. (b) Graphs (obtained from DLS results) comparing the surfactant capability of BCS and Dolapix. D_{10}, D_{50} and D_{90} are plotted in the inset on the right, indicating that alumina particles are more stable and dispersed when using BCS. (c) Graph showing the equilibrium adsorption capacity *vs* the initial concentration of BCS. The dashed line highlights the MAX concentration (100% adsorption of all molecules). (d) Adsorption isotherm fitted to the Langmuir model.

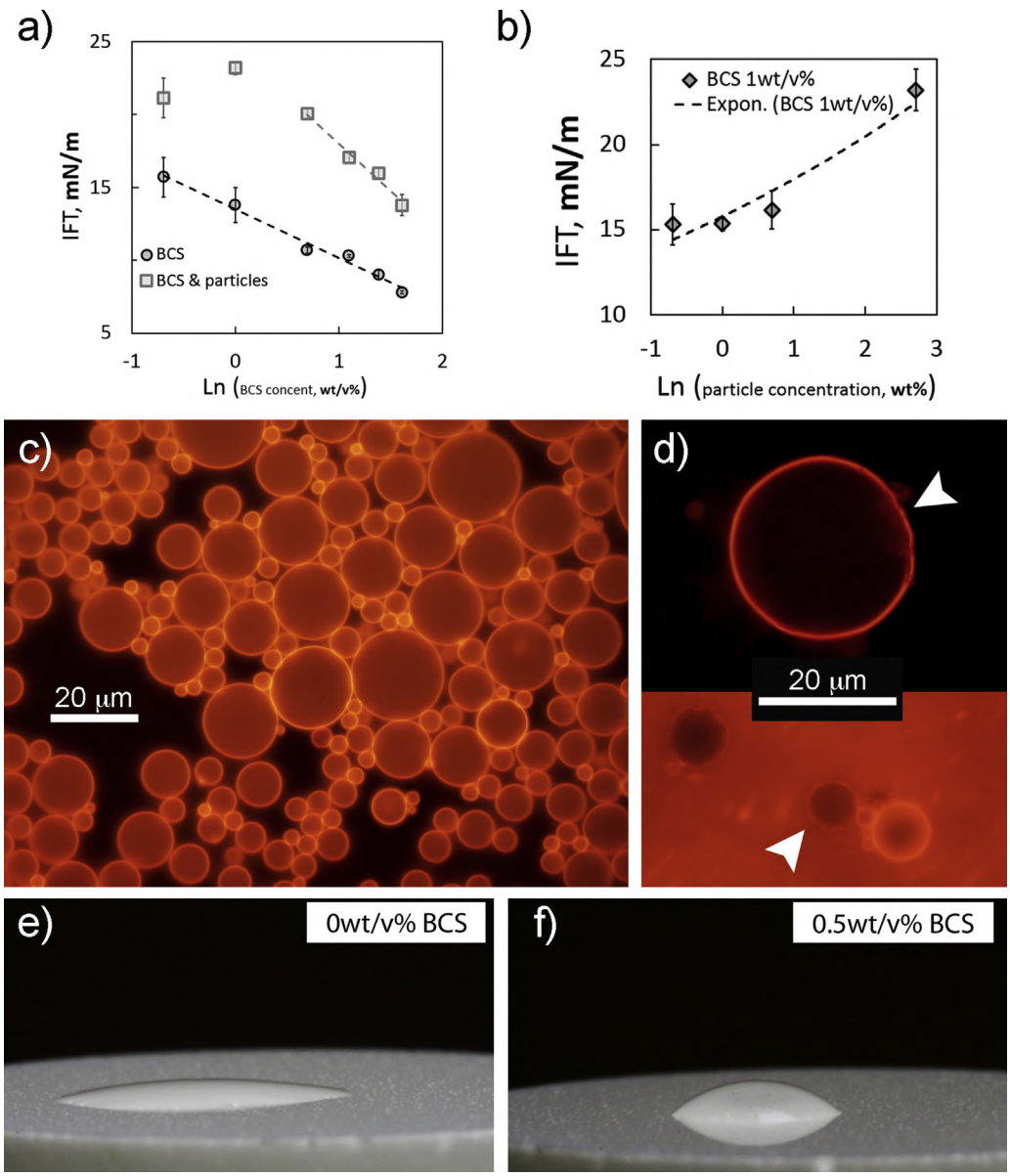

Fig. 3. Interface stabilisation in oil(decane)/water and oil(decane)/suspension emulsions. (a, b) IFT results from pendant drop experiments; (c, d) images taken with optical microscope using a rhodamine filter and (e, f) contact angle images also taken with an optical microscope using an 100× immersion occular. (a) Graph showing the effect of increasing BCS concentrations in IFT values (γl) for BCS solutions and the same solutions containing 17 vol% of alumina particles. IFT values decrease with increasing amounts of BCS whether there are particles or not in the continuous phase. In good agreement with the Gibbs isotherm, IFT results follow a linear trend with the Ln of the concentration in the bulk. (b) Interfacial tension exponentially increases with increasing particle concentrations (cp, wt%) for a fixed amount of BCS (1 wt/vol%). This proves that the role of particles in the stabilisation mechanism in the emulsion is not due to a reduction of the interfacial energy. (c) Image of a diluted oil/water emulsion (stabilised with BCSr) showing clearly how the BCS molecules concentrate at the oil/water interfaces. (d) Images of a diluted emulsified suspension (stabilised with BCSr) showing in detail the oil/water interface. A layer of fluorescent particles covers oil droplets (highlighted by arrows in the images), while the particles in the continuous phase move rapidly in Brownian motion (the image at the bottom was captured from a video; it illustrates this rapid movement in the continuous phase while the droplets remain still). (e, f) Contact angle of water on a clean and a BCS functionalised (0.5 wt%) alumina substrate.

alumina particles (positively charged at pH < 9 due to OH_2^+ groups on the alumina surface); 2) via ligand exchange reactions between the hydroxyl groups in the alumina surface (—OH or $—OH^{2+}$) and the carboxyl groups in the MAA branches (COO^-) [29,30] and 3) chemical covalent bonding between the carboxylic residues and the metal oxides on the surface of the particles that may be established during the ball milling process [31].

3.2. Emulsification

BCS molecules contain hydrophilic domains (MAA and PEGMA) and hydrophobic chain ends (DDT); it is an amphiphile at any pH value. The DDT chain ends provide multiple anchoring points to the decane droplets, which enables the emulsification of ceramic suspensions without any additional additive. BCS stabilises oil (decane, dispersed phase)/water interfaces by the attachment of hydrophobic DDT ends to the oil droplets, and the steric and electrostatic stabilisations (at pH > pK_a) provided by hydrophilic domains in the continuous phase (water or suspension). IFT results indicate that increasing concentrations of BCS (from 0.5 to 5 wt/vol%) reduce the interfacial energy of oil/water interfaces (Fig. 3a). Images of emulsions prepared with rhodamine modified BCS molecules (BCSr) demonstrate how they segregate at the interface of oil/water emulsions (Fig. 3c). The interfaces exhibit higher fluorescence than the

oil droplets and the continuous phase due to a higher concentration of BCSr at the interface (Fig. 3c). IFT values of suspension drops (BCS and particles) in decane are larger than the respective particle free BCS solutions. For a fixed amount of particles, IFT values decrease with increasing BCS concentrations (from 0.5 to 5 wt/vol%), and rise with larger amount of particles in the suspensions (from 0.5 to 17 vol%) for a constant amount of BCS (Fig. 3a, b). Fluorescence images of emulsified suspensions also show the segregation of BCSr at the interface (Fig. 3d) as well as a higher concentration of ceramic particles surrounding the oil droplets (inset in Fig. 3d). Live images show rapid Brownian motion of fluorescent particles in the continuous phase but also a tendency to segregate at the interface. Based on our observations with the microscope as well as our hands-on experience during the processing of the emulsions, we think that the BCS-functionalized particles have a very important role in stabilising the interface, leading to the well-known Pickering emulsions. According to our results, the alumina particles do not reduce the IFT at the oil/water interface (Fig. 3a, b). IFT values exponentially rise with particle content, evidencing that the mechanisms through which they contribute to overall emulsion stability are different. A previous work suggests that interfacial tension (IFT) reduction is not the operative stabilisation mechanism in Pickering emulsions, and points that the stabilising effects of the particles are related to steric hindrance or surface rheology effects [32]. The increase of γI with c_P (Fig. 3b) may be explained by rigidity of the emulsion "skin" due to particle surface crowding [32]. In addition, the repulsion forces between the BCS functionalized particles in the "skin" of a droplet with the particles in the "skin" of an adjacent one will contribute to avoid droplet coalescence and maintain a stable emulsion. We have also found that BCS increases the contact angle of water on alumina surfaces (Fig. 3e, f), which may increase the energy required to remove the functionalized particle from the oil/water interface [22,33]. It is highly likely that a combination of particle and surfactant (BCSr) stabilisation is taking place at the oil/water interface [12].

During the emulsification process with 50 vol% decane, we found that concentrated suspensions (43 vol% solids) require lower emulsification speeds (from 1000 to 10,000 rpm) to obtain stable emulsions. Under these conditions the crowd of BCS functionalised particles facilitate droplet breakup, creating a shell on the surface and avoiding coalescence; the emulsification takes place in the rupture controlled domain [22,34]. The parameters affecting the emulsification in this region are particle concentration and shear rate. Suspensions with high viscosity (43 vol%, Fig. 3a) favour droplet breakage under shear. A lower amount of particles in the suspensions strongly affects the emulsification, due to a lower viscosity of the continuous phase, and the decrease on the probability to hit the interface and surface coverage. This shifts the mixing conditions from the rupture controlled to the coalescence-controlled domain [22]. Emulsions prepared with low viscosity suspensions (7–25 vol%, Fig. 3a) are less stable, leading to creaming and phase separation within an hour when prepared at emulsification speeds below 10,000 rpm. An increase in stirring speed during emulsification up to 24,000 rpm facilitates breakage in smaller droplets, avoids creaming and provides stable emulsions for more than 24 h. When working with low solid loading suspensions (7–15 vol%), it is possible to obtain either a very stable emulsion in the rupture-controlled domain at high stirring speed (up to 24,000 rpm), or emulsions with limited stability in the coalescence-controlled domain at low speed (2000 rpm). Emulsifying conditions determine droplet size and distribution. For example, high stirring velocities (10,000 rpm) and particle contents (43 vol%) lead to very small droplets (down to 1 μm). By changing solid loading and emulsification speed, we can change the morphology of the emulsions, allowing us to manipulate the soft template that will eventually shape the final ceramic structures.

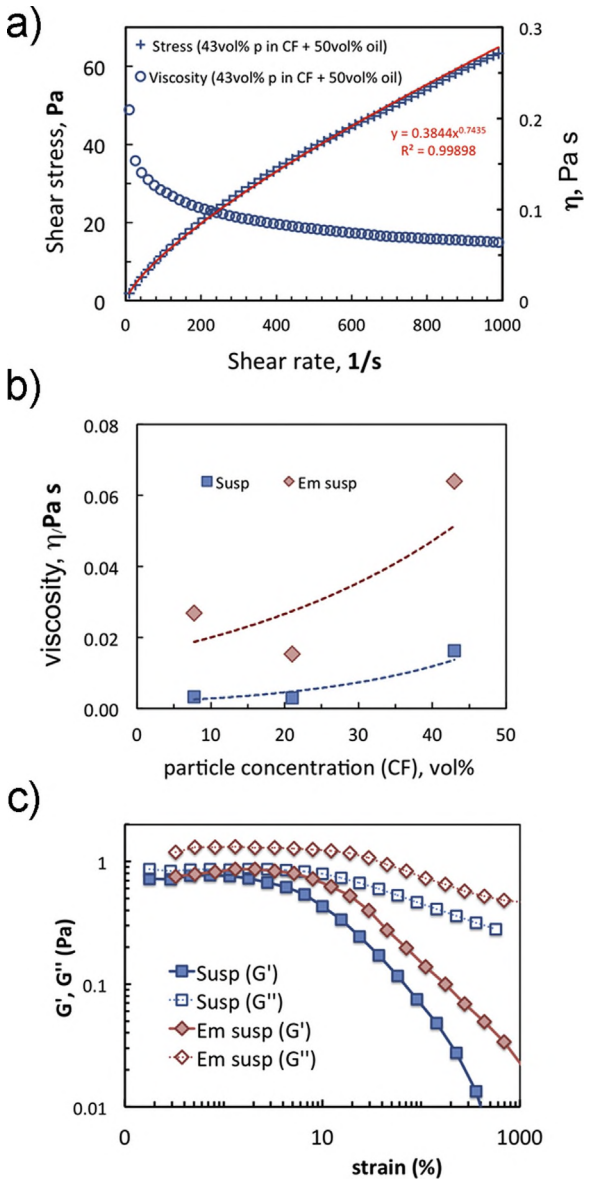

Fig. 4. (a) Example of flow behaviour for an emulsion with 43 vol% particles in the continuous phase prepared with 50 vol% oil. Viscosity (b) and viscoelastic fingerprints (c) for suspensions and emulsified suspensions. (b) Graph showing the effect of particle concentration of the continuous phase (CF) in viscosity values. BCS stabilised suspensions have a Newtonian behaviour, low particle concentrations up to 20 vol% do not have a noticeable effect on viscosity, but high solid loading (43 vol%) increases the viscosity substantially. (c) Viscoelastic fingerprints (amplitude sweep at 1 Hz) for a 43 vol% suspension (Susp) and a emulsified suspension containing the same amount of solids in the continuous phase (Em susp).

3.3. *Rheology of suspensions and emulsions*

Alumina suspensions stabilised with BCS at pH 8 have linear flow behaviour. Their viscosities increase with solid contents (Fig. 4b). Suspensions with particle concentrations up to 21 vol% show similar viscosity values, but the viscosity increases at higher solid loadings (Fig. 4b). When these suspensions are emulsified with 50 vol% of oil, their behaviour becomes slightly shear thinning with higher viscosities (Fig. 4a, b). Suspensions and emulsions are both complex fluids containing alumina particles, BCS molecules as well as oil droplets (in the emulsions). They all have an effect on rheolog-

ical behaviour. At rest, BCS molecules are organised in random coils, particles move randomly in Brownian motion in the continuous phase in between oil droplets with spherical shape leading to higher viscosities and yield stresses. Under shear, particles flow in the same direction, random coils will elongate and emulsion droplets will deform and orient in flow direction resulting in shear thinning behaviour. Viscoelastic fingerprints for suspensions and emulsions with high solid loading (43 vol%) show similar behaviours (Fig. 4b). Both exhibit a linear viscosity region (LVR) at strains under 10%, and the viscous component dominates ($G'' > G'$) within all the strain range measured (from 0.1 up to 1000%) with values of $G' \sim 0.7$ Pa and $G'' \sim 0.9$ Pa for the suspension and $G' \sim 0.8$ Pa and $G'' \sim 1.3$ Pa for the emulsion. G' and G'' are slightly bigger for the emulsified suspension probably due to droplet interactions and shape deformation during flow.

3.4. Directed assembly

Rheology also provides a valuable insight into the dispersed-to-aggregated phase transition by measuring the viscoelastic properties (elastic (storage, G') and viscous (loss, G'')) over time immediately after triggering the pH drop (Fig. 5). There is a rapid increase in both G'' and G', the crossover point ($G' > G''$) takes place within minutes for all suspensions and emulsions, and then both rapidly increase until they stabilise to eventually reach a plateau. At this point, there is a strong binding effect due to hydrogen bonding across BCS molecules that connect a stiff particle network. Comparing the viscoelastic fingerprints before and after aggregation (Fig. 6a), we find that the storage modulus (G') dominates and increases up to 5 orders of magnitude after aggregation. The viscoelastic fingerprint also shows how this stiff particle network breaks down (G', and G'' decrease and G'' dominates) at strains of ~10% (Fig. 6a).

We find that aggregation kinetics slightly differs for suspensions and emulsified suspensions (Fig. 5). For the latter, the viscoelastic properties (G' and G'') increase at different rates during the network establishment, which might be associated with shrinkage. It takes place due to the packing of particles in a BCS network that is accompanied by small amounts of sweating (water segregation). For a 43 vol% suspension, shrinkage is detected within 3 min (Fig. 5a). In the emulsion it is a bit more delayed (~6 min), taking place simultaneously with the change of increasing rate for the viscoelastic moduli (Fig. 5b). This could be explained by the need of a stiff particle network in the continuous phase that must be strong enough to bring together and pack particles and oil droplets during shrinking. Other factors that also change the kinetics are pH (i.e. amounts of pH trigger (GδL)), BCS and particle concentrations and temperature. The pH (GδL concentration) plays the main role in the kinetics and stiffness of the assembly; it is responsible for the establishment of multiple non-covalent interactions across BCS molecules that connect the particles in a stiff network. An increase of BCS concentrations leads to longer aggregation times due to its buffer role, which slows down the pH drop. For a fixed amount of BCS and particles, an increase on the amount of GδL results in larger G' values as well as shorter times to crossover point ($G' > G''$) and final plateau (Fig. 6c). GδL amounts above 2 wt/vol% lead to fast aggregation times (<2 min) for concentrated suspensions (43 vol%, containing 1 wt/vol% BCS) facilitating a rapid assembly. As soon as the pH drops, the particle network forms when the hydrogen bonds are 'turned on'. For the emulsified suspensions, higher concentration of particles in the continuous phase leads to faster aggregation kinetics and stiffer self-supporting green bodies (Fig. 6b, d). Temperature also affects the kinetics; triggering the aggregation in an ice bath slows down GδL hydrolysis to gluconic acid and as a consequence delays the network establishment.

3.5. Consolidation: processing map

Directing the assembly of suspensions and emulsions into complex shape moulds enables the fabrication of intricate ceramic components [12]. After consolidation at high-temperature, they can have densities ranging from 99% to 10% by using suspensions or emulsified suspensions. The aggregation of suspensions leads to high-density pieces (up to 99%, Table 1), while the emulsifica-

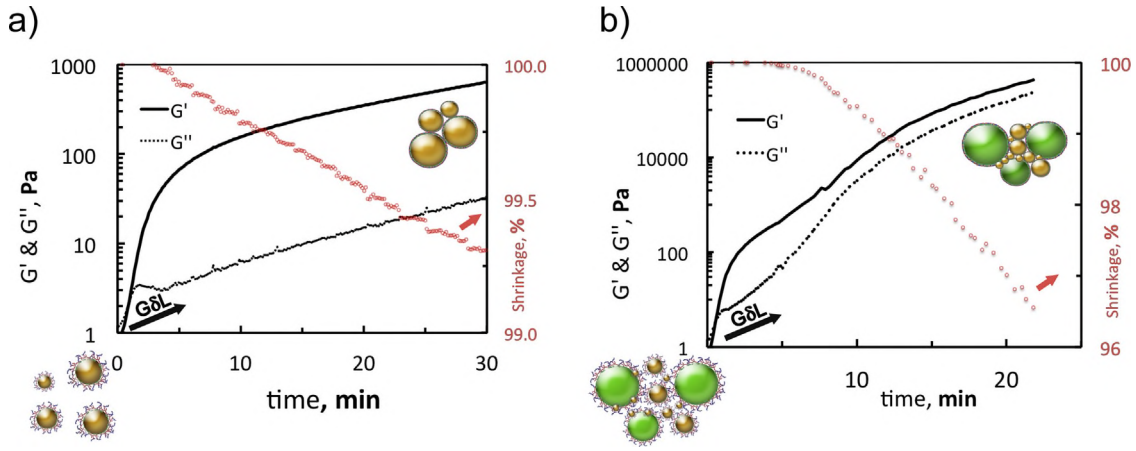

Fig. 5. Examples of network establishment under different conditions for (a) 43 vol% alumina suspension mixed with 1 wt/vol% GδL, and (b) emulsified suspension containing 43 vol% alumina in the continuous phase mixed with 2 wt/vol% GδL. Both measured using a time sweep at fixed frequency and angular displacement (1 Hz, 5×10^{-5} rad).

Table 1
Mechanical properties of dense alumina parts prepared from a suspension containing 43 vol% alumina particles with 2 wt/vol% BCS and 1 wt/vol% GδL. Drying conditions: 90 min under vacuum (0.6 bar) followed by 48 h at room temperature (demoulding after only 24 h) and final step at 40 °C under forced convection.

Density	Relative density	Vickers Hardness	Fracture toughness[a]	Strength (4pb)[b]	Strength of green body (4pb)
3.90 ± 0.01 g/cm^3	98.7 ± 0.2%	1598 ± 78 HV	4.78 ± 0.64 MPa $\sqrt{m}$	194 ± 45 MPa	454 ± 176 kPa

[a] ASTM C1421-10.
[b] ASTM C1161-02c.

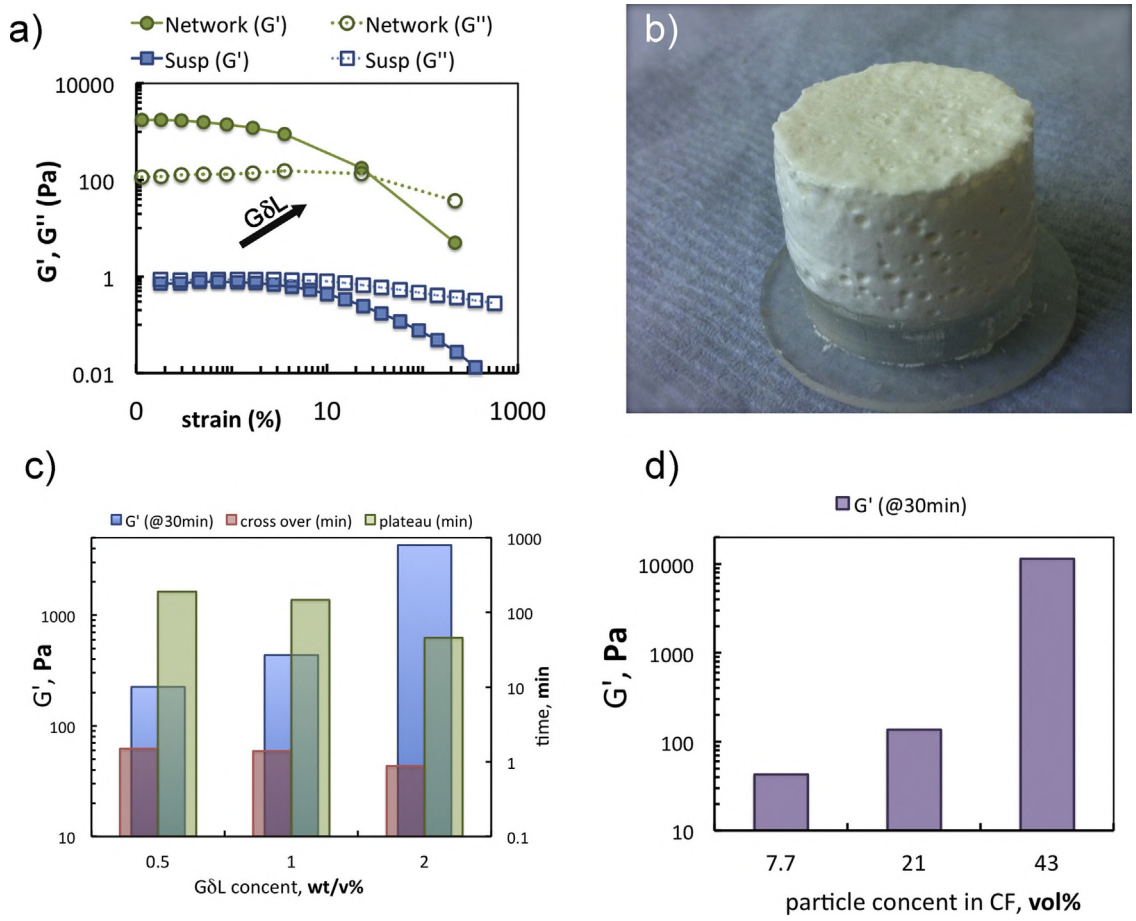

Fig. 6. (a) Viscoelastic fingerprint showing the change in the magnitude of viscoelastic moduli before and after aggregation ('susp' corresponds to a 43 vol% alumina suspension and 'network' to the same after adding 1 wt/vol% GδL). (b) Image of a self-supporting emulsified suspension after aggregation containing 21 vol% particles in the continuous phase. (c) GδL role in the aggregation kinetics and network stiffness (43 vol% alumina suspensions, stabilised with 2 wt/vol% BCS). Increasing the pH trigger concentration leads to an increase of G′ (values measured at 30 min after adding GδL), a reduction of time to cross over point (where the transition from liquid-like to solid-like behaviour takes place, G′ > G″) and to reach the final plateau in G′ and G″ values. (d) Histogram showing the increase of network stiffness (G′) with the amount of particles in the continuous phase (CF) for emulsified suspensions (G′ values measured at 30 min, fixed amounts of GδL (2 wt/vol%) and BCS (1 wt/vol%)).

tion step opens up multiple possibilities offering a wide variety of porous microstructures (Figs. 7–9). The relation between emulsifying conditions, particle concentration in the continuous phase and final microstructures after consolidation is summarised in a processing map (Fig. 7).

By assembling emulsions prepared at relatively low emulsification speeds (~2000 rpm) with high solid loading we obtain closed cell ceramic structures with porosities of 50–60% and an average pore size of 33 ± 13 μm (Figs. 7 and 8a). Increasing the stirring speed during emulsification (up to 10,000 rpm) results in a considerable droplet size reduction that lead to a very small pore size in the final structure, with more interconnected porosity (total 60%, 37% open) and an average of 4 ± 1.5 μm with all the pores under 10 μm (Figs. 7 and 8b). Sintering of these samples must be limited to 0.5 h to preserve the microstructure and avoid the fusion of the pore walls and loss of porosity.

Emulsified suspensions with low particle concentrations (7–15 vol% in CF) prepared with stirring speeds (up to 10,000 rpm), tend to cream, coalesce and destabilize within an hour. But adding GδL amounts up to 12 wt/vol% quickly accelerates the aggregation kinetics and preserves the droplet arrangement before destabilization takes place. This makes it possible to obtain unique graded structures with large interconnected pores at the top and in decreasing size towards the bottom (Fig. 9) [12]. Increasing the emulsification speed up to 24,000 rpm leads to more

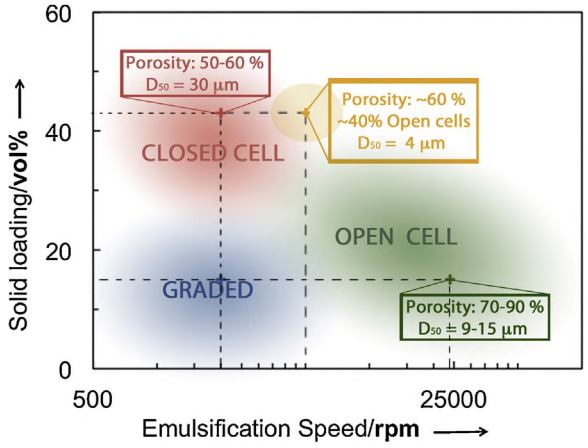

Fig. 7. Map illustrating the correlation between particle concentration in CF, stirring speed during the emulsifying process and final structural properties of porous alumina (porosity, interconnectivity and pore size). Particle concentrations in CF range from 7 to 43 vol% and stirring speeds between 1000 and 24,000 rpm. Higher particle concentrations lead to closed porosity, with smaller pore sizes with increasing emulsification speeds. Lower particle concentrations lead to higher and more interconnected porosities.

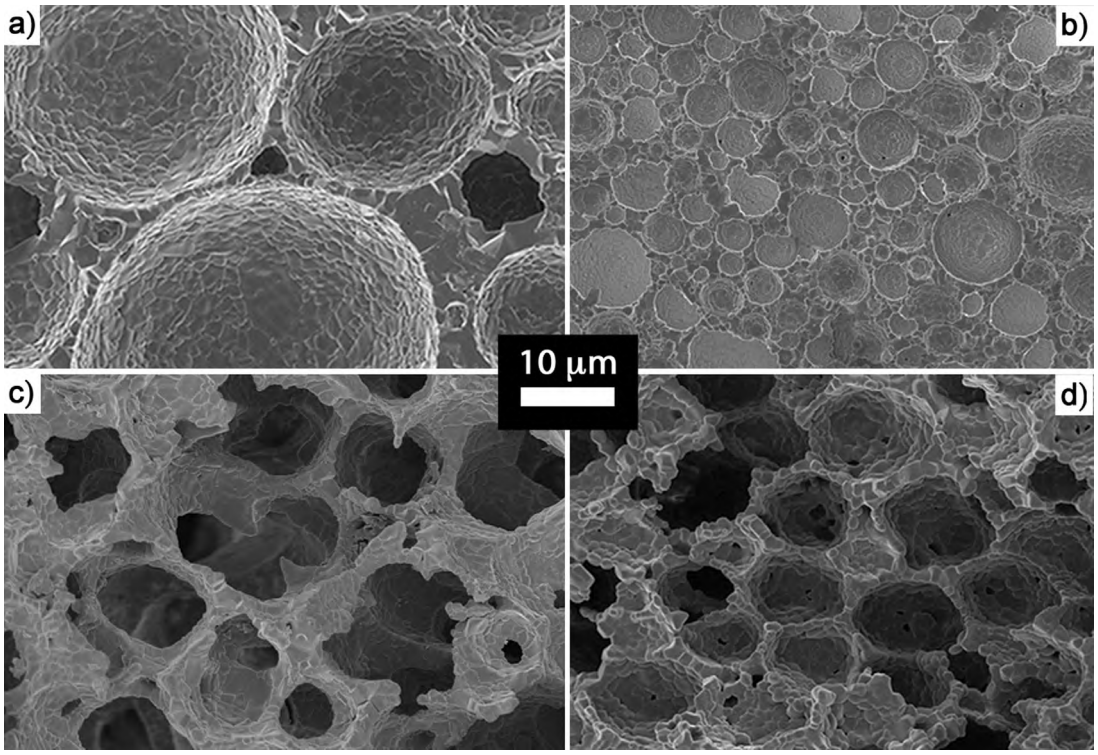

Fig. 8. Range of microstructures after consolidation starting from emulsified suspension with (a, b) 43 vol%, (c) 15 vol% and (d) 12 vol% alumina particles in CF. Sintered for 1 h (a, c and d) and (b) 0.5 h at 1550 °C. (a) High solid loading results in closed cell macro porous alumina with high density walls and struts. (b) Increasing the stirring speed up to 10,000 rpm reduces the final average pore size to ~4 μm with some pores over 1 μm. (c) When using suspensions with lower concentrations we obtain open cell foams with higher porosity and thinner walls, with a nicely interconnected structure. (d) Samples subjected to slow drying at room temperature in air display pores with polyhedral shapes (resembling a honeycomb) due to the formation of thin films as oil droplets in the emulsion tend to coalesce over time.

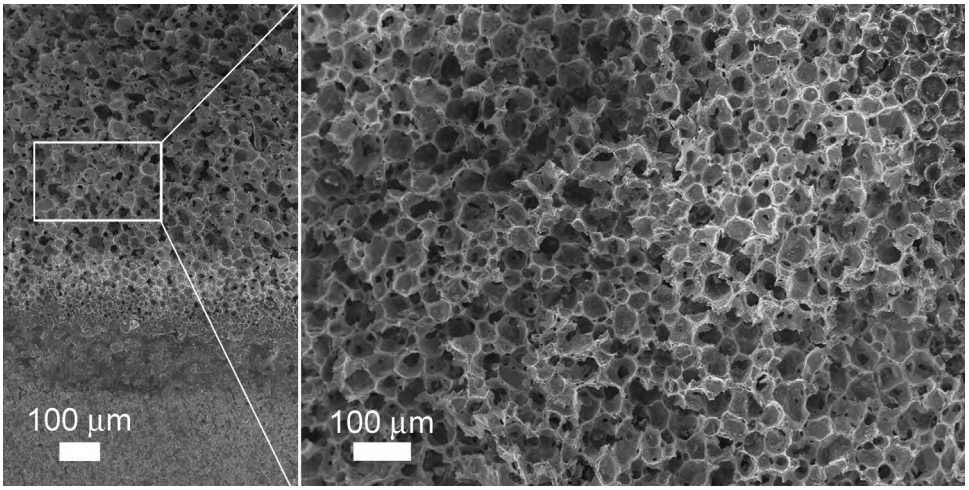

Fig. 9. SEM images of porous alumina with gradient porosity obtained from an emulsified suspension with limited stability (GRADED region in the processing map (Fig. 7)), corresponding to low solid loading (12 vol%) and low emulsification speed (<8000 rpm). In these emulsions, particles that do not hit droplet surfaces sediment at the bottom, followed by small and stable oil droplets covered by particles on their surfaces, bigger droplets are less stable tending to coalesce and separate at the top. A rapid assembly of these emulsions preserves this arrangement and provides unique graded structures.

stable emulsions, which after consolidation result in a homogeneous microstructure with interconnected porosity (average of 78% porosity, 73% open cell) and average pore size of 18 ± 6 μm (Figs. 7 and 8c). Longer emulsification times (> 5mins) and very slow drying at room temperature in air enables the formation of honeycomb like structures with thin walls, porosities up to 80% (69% open cell) and average pore size of 9 ± 3 μm (Figs. 7 and 8d)[12].

3.6. Characterisation

The mechanical performance of high-density ceramic parts is intimately related with processing conditions and drying is a critical step in advanced ceramics. Being our goal to provide a new approach to control the architecture of ceramic structures, it is essential to understand how drying may affect them to minimize

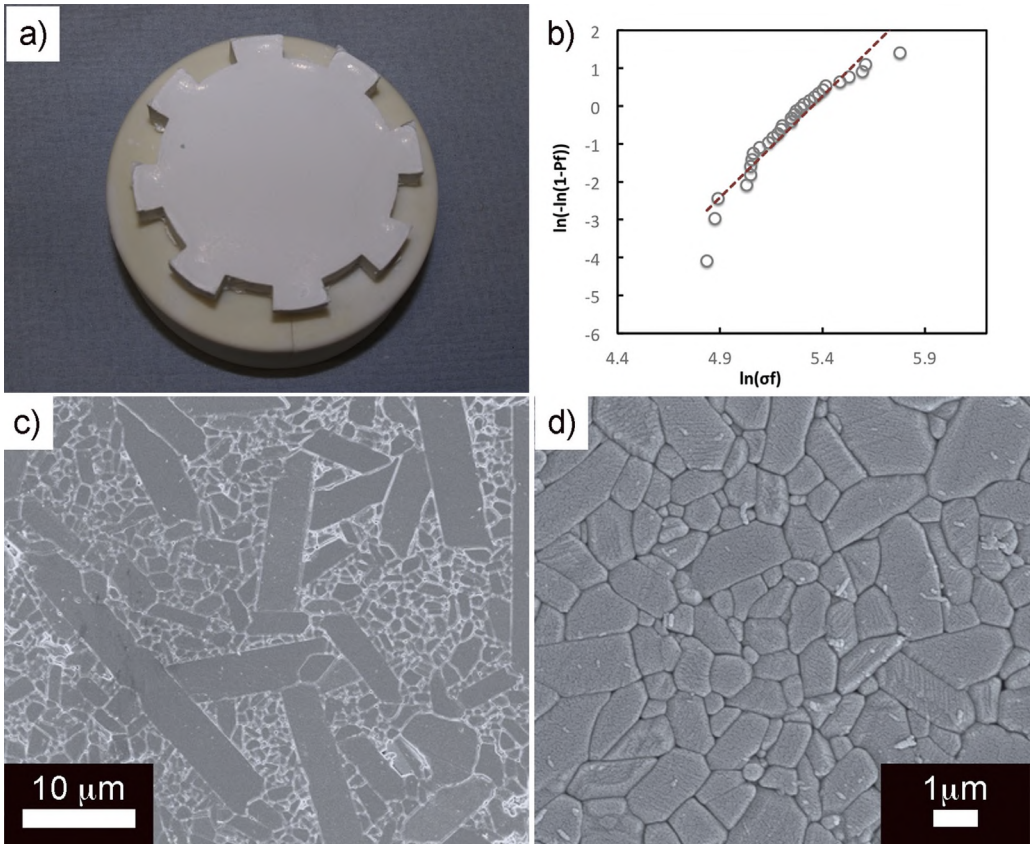

Fig. 10. Dense ceramic components prepared with 43 vol% alumina suspensions (2 wt/vol% BCS, and 1 wt/vol% GδL). (a) Image of a high-density mixing blade. (b) Weibull distribution plot obtained after testing 30 specimens in 4 point bending following the ASTM standard C1161-02c. (c) and (d) SEM images showing the microstructure. Grains show good contact along the materials with no inter granular porosity. The microstructure exhibits abnormal grain growth that results in higher toughness.

its detrimental effects. The highest density microstructures are achieved when drying of suspensions takes place in three steps (see Section 2, Fig. 10). The final parts have average strengths of 194 MPa but a relatively low Weibull number of 5.4 (Table 1, Fig. 10). Their fracture toughness is on the high range for dense alumina materials (Table 1). The materials have dense microstructure with no intergranular porosity, but the SEM images also reveal abnormal grain growth (average aspect ratio of 3.42 ± 1.00, Fig. 10c, d). This could be caused by impurities from the environment during processing as well as leftover S from the BCS molecules, and Na from the solutions used to prepare the materials [35]. These elongated grains (that can measure up to 70 μm in length) are probably responsible for increased toughness [36]. From the toughness and strength values the critical defect size is of the order of ~100 μm. This suggests that relatively big pores remain in some samples – probably due to trapped gas bubbles – increasing the probability of fracture when the pore is in the region under stress and decreasing reliability. Longer degasification times and the use of sintering additives (MgO or ZrO_2) to inhibit abnormal grain growth, could improve the microstructures and their mechanical performance.

In a previous communication, we reported the mechanical properties of porous alumina with porosities between 50 and 80% [12]. Crushing strengths are particularly high for closed cell structures with porosities between 50 and 60% [12]. Here, we provide additional data that confirm our preliminary results. All the structures have a clear breaking point; the curves exhibit an initial linear elastic behaviour until they reach the critical crushing strength (values used to calculate the compressive strengths), typical of elastic brittle foams. After that the stress drops, followed by a plateau and densification upon further compression (Fig. 11a). We find that the crosshead speed during compression tests does not significantly affect the results (Fig. 11b). SEM images of dried specimens before consolidation reveal how the hierarchical arrangement at the nano and micro scale is likely responsible for the excellent mechanical performance in compression. The low viscosity of the alumina suspensions at pH 8 throughout the highly organised soft template facilitates very efficient packing in the continuous phase. This arrangement is preserved when the pH drops and BCS molecules change behaviour to binding mode forming a particle network across continuous phase and interfaces. The wall of a pore before sintering shows how the particles perfectly arrange at the oil/water interface (Fig. 12a, b). This arrangement provides high-density walls and struts after consolidation (Fig. 12c, d). Abnormal grain growth also takes place in these porous structures.

Their mechanical behaviour in bending seems to follow the trend of other macro-porous alumina materials in literature [38,46] (Fig. 13) and also the theoretical predictions using Gibson and Ashby model. All the specimens show a brittle fracture after linear elastic behaviour (Fig. 13a), with bending strength decreasing when porosity increases. Our results show how bending strengths can be overestimated when using 3pb. The average bending strength decreases around 50% when determined in 4pb (Fig. 13) because the larger region under stress increases the probability of failure. BCS concentrations seem to have an important role in mechanical performance. Bending strengths for samples with similar porosities (54 and 51%) decrease substantially with BCS content in the suspension. Increasing BCS concentration from 1 to 2 wt/vol% BCS results in a drop of 46% in average bending strength in 3pb, and 51% in 4pb. The formation of small pores in the walls and windows interconnecting the structure leads to an increase of open porosity that seems to be responsible for failure at lower strengths (Fig. 13). These results provide very important information to take

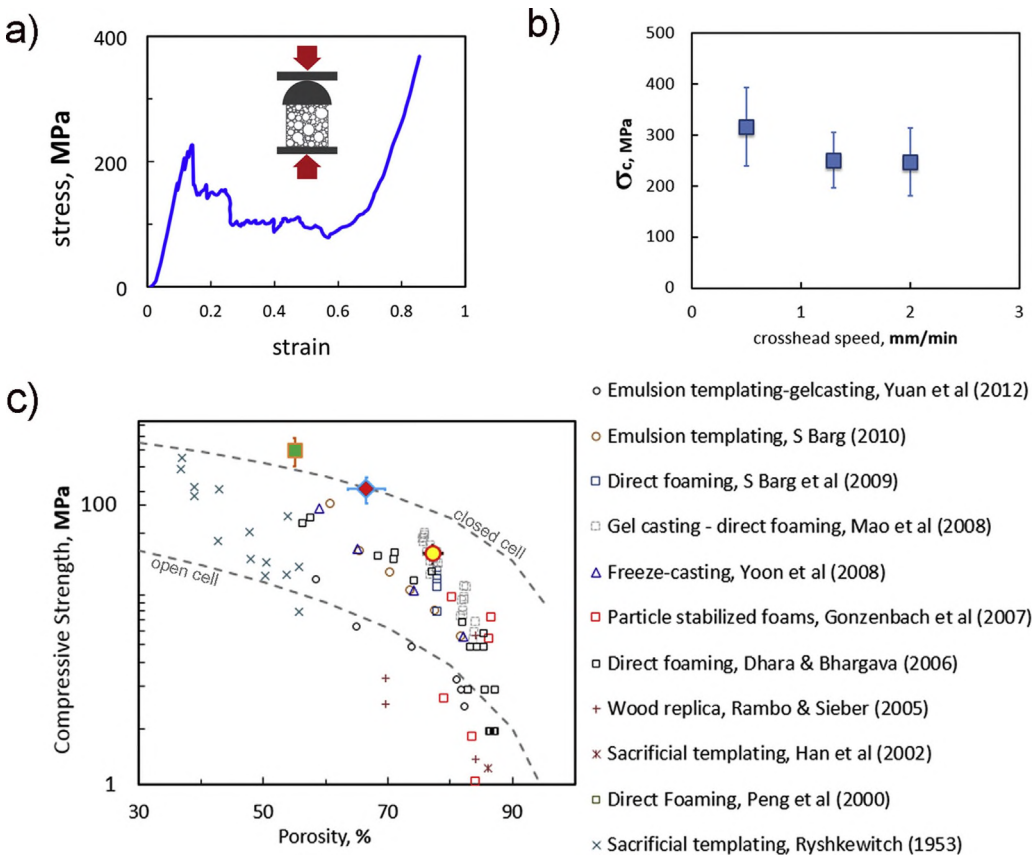

Fig. 11. (a) Stress-strain curve; (b) effect of crosshead speed on crushing strength; and (c) comparison of compressive strength of three materials with porosities of ~54, 68 and 78% with other macroporous materials in literature [17,34,37–45]. Closed cell porous alumina (~54%) exhibits a remarkable high strength in compression compared to other materials and the Gibson and Ashby model (dashed lines for this model considering strength of the wall of 400 MPa). As porosity increase and pores are more interconnected and walls get thinner, the crushing strength drops.

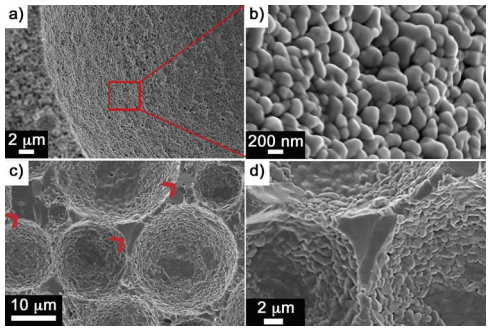

Fig. 12. SEM images showing the structural features in walls and struts before (a, b) and after sintering (c, d) for a porous structure prepared with an emulsified suspension containing 43 vol% particles and 1 wt/vol% BCS. (a, b) particle arrangement in the continuous phase and at the oil/water interface before sintering at 1550 °C. (c, d) Images showing high density struts after sintering. Abnormal grain growth can also be observed in the porous sample (arrows).

into account in the manufacturing of porous materials using this approach.

4. Conclusions

Complex alumina parts with a wide range of microstructures – from high-density (~99 th%) to porosities up to ~80%- can be prepared using a responsive building blocks approach. Using small amounts of a pH responsive branched copolymer we have been able to functionalised ceramic particles and prepared very stable water based suspensions. Particle size and adsorption measurements confirm the functionalization of alumina surfaces with very small amounts of BCS (1 wt/vol%). The emulsification of these suspensions results in very stable Pickering emulsions that act as a template to create complex ceramic components with hierarchical structures. The suspensions have linear flow behaviour while the emulsions deviate from Newtonian behaviour and become shear thinning. Their viscosities increase with solid loading. Both are aggregated into particle networks by the action of a pH trigger (GδL) that drops the pH below the pKa of BCS. This rapidly increases the viscosity and magnitude of the viscoelastic moduli (G′ and G″) leading to 'pseudo-gels'. The kinetics of this transition and strength of the particle networks can be manipulated by tuning different parameters (solid loading, amounts of BCS and GδL, temperature). One of the advantages of the responsive particles approach is that we can pour the suspensions and emulsions into intricate moulds when their viscosity is very low, immediately after triggering the aggregation with GδL. This also facilitates an efficient packing of the particles and soft templates leading to very well organised microstructures. Emulsification conditions play a critical role in the microstructure of the macroporous alumina structures. By adjusting solid loading in the continuous phase, energy applied during emulsification and amounts of GδL we can obtain closed cell structures with remarkable strengths in compression (up to 400 MPa for a porosity of 55%) to open cell and highly interconnected materials with porosities up to 80%. Their bending strength in 4pb (~40 MPa for 50–55% porosity) follows the trend of other materials in literature. The flexibility of the approach also enables the preparation of

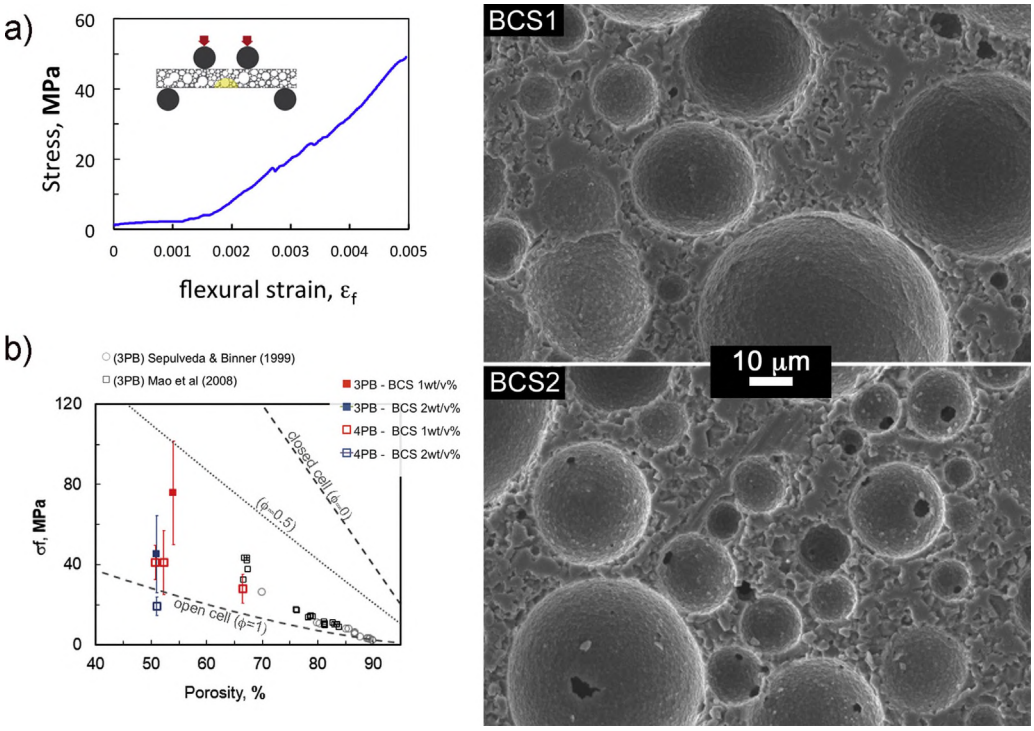

Fig. 13. (a) Example stress vs. strain curve during bending for one of the specimens. (b) Graph showing bending strength of alumina macro porous structures including data from this work and [38,46]. Dashed and dotted lines highlight the Gibson and Ashby theoretical predictions calculated considering the strength of the dense materials in this work fabricated using the same process (~400 MPa in 4pb).

high-density alumina components with average strengths in 4pb of ~200 MPa. The best microstructures are obtained when the aggregation takes place under vacuum to help with bubble elimination, and drying is carried out in three stages. In short, the use of a responsive polymer designed for drug delivery (BCS) to design responsive building blocks in ceramic processing opens up multiple possibilities to assemble complex structures. We can formulate a wide range of water-based soft materials with promising potential in different manufacturing techniques, from casting, templating to 3D printing. An additional advantage is that waste production can be minimised thanks to the reversibility of the assembly process.

Acknowledgements

EGT would like to acknowledge the EPSRC Grant graphene 3D networks (EP/K01658X/1). SB would like to thank the European Commission (FP7—Marie Curie Intra European Fellowship ACIN). GM would like to acknowledge the European Commission funding under the 7th Framework Programme (Marie Curie Initial Training Networks; grant number: 289958, Bioceramics for Bone Repair). The authors would also like to acknowledge the support of RFEC-ATL, ONRG and DARPA.

References

[1] B. Jeong, A. Gutowska, Lessons from nature: stimuli-responsive polymers and their biomedical applications, Trends Biotechnol. 20 (2002) 305–311.
[2] C. de las Heras Alarcón, S. Pennadam, C. Alexander, Stimuli responsive polymers for biomedical applications, Chem. Soc. Rev. 34 (3) (2005) 276–285.
[3] M.A.C. Stuart, W.T.S. Huck, J. Genzer, M. Müller, C. Ober, M. Stamm, et al., Emerging applications of stimuli-responsive polymer materials, Nat. Mater. 9 (2010) 101–113.
[4] S. Seiffert, Small but smart: sensitive microgel capsules, Angew. Chem. Int. Ed. 52 (44) (2013) 11462–11468.
[5] P. Brown, C.P. Butts, J. Eastoe, Stimuli-responsive surfactants, Soft Matter 9 (2013) 2365–2374.
[6] N. Nath, A. Chilkoti, Creating smart surfaces using stimuli responsive polymers, Adv. Mater. 14 (2002) 1243–1247.
[7] S. Barg, M.D.M. Innocentini, R.V. Meloni, W.S. Chacon, H. Wang, D. Koch, et al., Physical and high-temperature permeation features of double-layered cellular filtering membranes prepared via freeze casting of emulsified powder suspensions, J. Membr. Sci. 383 (2011) 35–43.
[8] A.R. Studart, U.T. Gonzenbach, E. Tervoort, L.J. Gauckler, Processing routes to macroporous ceramics: a review, J. Am. Ceram. Soc. 89 (2006) 1771–1789.
[9] P. Colombo, Conventional and novel processing methods for cellular ceramics, Philos. Trans. R. Soc. A: Math. Phys. Eng. Sci. 364 (2006) 109–124.
[10] E. Munch, M.E. Launey, D.H. Alsem, E. Saiz, A.P. Tomsia, R.O. Ritchie, Tough bio-inspired hybrid materials, Science 322 (2008) 1516–1520.
[11] U.T. Gonzenbach, A.R. Studart, E. Tervoort, L.J. Gauckler, Ultrastable particle-stabilized foams, Angew. Chem. Int. Ed. 45 (2006) 3526–3530.
[12] E. García-Tuñon, S. Barg, R. Bell, J.V.M. Weaver, C. Walter, L. Goyos, et al., Designing smart particles for the assembly of complex macroscopic structures, Angew. Chem. Int. Ed. 52 (2013) 7805–7808.
[13] A.R. Studart, U.T. Gonzenbach, I. Akartuna, E. Tervoort, L.J. Gauckler, Materials from foams and emulsions stabilized by colloidal particles, J. Mater. Chem. 17 (2007) 3283–3289.
[14] A.R. Studart, A. Nelson, B. Iwanovsky, M. Kotyrba, A.A. Kündig, F.H. Dalla Torre, et al., Metallic foams from nanoparticle-stabilized wet foams and emulsions, J. Mater. Chem. 22 (2011) 820–823.
[15] I. Akartuna, A.R. Studart, E. Tervoort, L.J. Gauckler, Macroporous ceramics from particle-stabilized emulsions, Adv. Mater. 20 (2008) 4714–4718.
[16] S. Barg, B.P. Binks, H. Wang, D. Koch, G. Grathwohl, Cellular ceramics from emulsified suspensions of mixed particles, J. Porous Mater. 19 (2011) 859–867.
[17] S. Barg, E.G. de Moraes, D. Koch, G. Grathwohl, New cellular ceramics from high alkane phase emulsified suspensions (HAPES), J. Eur. Ceram. Soc. 29 (2009) 2439–2446.
[18] V.O. Ikem, A. Menner, A. Bismarck, High internal phase emulsions stabilized solely by functionalized silica particles, Angew. Chem. Int. Ed. 47 (2008) 8277–8279.
[19] V.O. Ikem, A. Menner, T.S. Horozov, A. Bismarck, Highly permeable macroporous polymers synthesized from pickering medium and high internal phase emulsion templates, Adv. Mater. 22 (2010) 3588–3592.
[20] H. Zhang, A.I. Cooper, Synthesis and applications of emulsion-templated porous materials, Soft Matter 1 (2005) 107–113.
[21] S.U. Pickering, CXCVI.—emulsions, J. Chem. Soc., Trans. 91 (1907) 2001–2021.
[22] P.N. Sturzenegger, U.T. Gonzenbach, S. Koltzenburg, L.J. Gauckler, Controlling the formation of particle-stabilized water-in-oil emulsions, Soft Matter 8 (2012) 7471–7479.
[23] I. Akartuna, E. Tervoort, J.C.H. Wong, A.R. Studart, L.J. Gauckler, Macroporous polymers from particle-stabilized emulsions, Polymer 50 (2009) 3645–3651.
[24] J.V.M. Weaver, S.P. Rannard, A.I. Cooper, Polymer-mediated hierarchical and reversible emulsion droplet assembly, Angew. Chem. Int. Ed. 121 (2009) 2165–2168.

[25] E. García-Tuñon, S. Barg, J. Franco, R. Bell, et al., Printing in three dimensions with graphene, Adv. Mater. 10 (2015) 1688–1693.
[26] J.V. Weaver, D.J. Adams, Synthesis and application of pH-responsive branched copolymer nanoparticles (PRBNs): a comparison with pH-responsive shell cross-linked micelles, Soft Matter 6 (2010) 2575–2582.
[27] R.T. Woodward, C. Hight, U. Yildiz, N. Schaeffer, E.M. Valliant, J.R. Jones, et al., Reversible aggregation of responsive polymer-stabilized colloids and the pH-dependent formation of porous scaffolds, Soft Matter 7 (2011) 7560–7566.
[28] P. Zhang, L. Wang, Extended Langmuir equation for correlating multilayer adsorption equilibrium data, Sep. Purif. Technol. 70 (2010) 367–371.
[29] P.C. Hidber, T.J. Graule, L.J. Gauckler, Influence of the dispersant structure on properties of electrostatically stabilized aqueous alumina suspensions, J. Eur. Ceram. Soc. 17 (2–3) (1997) 239–249.
[30] A.R. Studart, E. Amstad, L.J. Gauckler, Colloidal stabilization of nanoparticles in concentrated suspensions, Langmuir 23 (2007) 1081–1090.
[31] M.E. Karaman, D.A. Antelmi, R.M. Pashley, The production of stable hydrophobic surfaces by the adsorption of hydrocarbon and fluorocarbon carboxylic acids onto alumina substrates, Colloids Surf. A 182 (2001) 285–298.
[32] E. Vignati, R. Piazza, T.P. Lockhart, Pickering emulsions: interfacial tension, colloidal layer morphology, and trapped-particle motion, Langmuir 19 (2003) 6650–6656.
[33] R. Aveyard, B.P. Binks, J.H. Clint, Emulsions stabilised solely by colloidal particles, Adv. Colloid Interface Sci. 100–102 (2003) 503–546.
[34] S. Barg, Cellular Ceramics Via Alkane Phase Emulsified Powder Suspensions (PhD Thesis), Shaker Verlag GmbH, Germany, 2010.
[35] I.J. Bae, S. Baik, Abnormal grain growth of alumina, J. Am. Ceram. Soc. 80 (5) (1997) 1149–1156.
[36] Z. Xie, J. Lu, T. Liu, Y. Huang, Y.B. Cheng, Fabrication of high toughness alumina with elongated grains, J. Mater. Sci. Lett. 20 (2001) 1425–1427.
[37] B. Yuan, H. Wu, X. Sun, G. Wang, H. Li, Fabrication of porous alumina green bodies from suspension emulsions by gelcasting, Mater. Lett. 81 (2012) 151–154.
[38] X. Mao, S. Shimai, S. Wang, Gelcasting of alumina foams consolidated by epoxy resin, J. Eur. Ceram. Soc. 28 (2008) 217–222.
[39] B.H. Yoon, W.Y. Choi, H.E. Kim, J.H. Kim, Y.H. Koh, Aligned porous alumina ceramics with high compressive strengths for bone tissue engineering, Scr. Mater. 58 (2008) 537–540.
[40] U.T. Gonzenbach, A.R. Studart, E. Tervoort, L.J. Gauckler, Macroporous ceramics from particle-stabilized wet foams, J. Am. Ceram. Soc. 90 (2007) 16–22.
[41] S. Dhara, P. Bhargava, Influence of slurry characteristics on porosity and mechanical properties of alumina foams, Int. J. Appl. Ceram. Technol. 3 (2006) 382–392.
[42] C.R. Rambo, H. Sieber, Novel synthetic route to biomorphic Al_2O_3 ceramics, Adv. Mater. 17 (2005) 1088–1091.
[43] Y.S. Han, J.B. Li, Q.M. Wei, K. Tang, The effect of sintering temperatures on alumina foam strength, Ceram. Int. 28 (2002) 755–759.
[44] H.X. Peng, Z. Fan, J. Evans, Factors affecting the microstructure of a fine ceramic foam, Ceram. Int. 26 (2000) 887–895.
[45] E. Ryshkewitch, Compression strength of porous sintered alumina and zirconia, J. Am. Ceram. Soc. 36 (1953) 65–68.
[46] P. Sepulveda, F.S. Ortega, M.D. Innocentini, V.C. Pandolfelli, Properties of highly porous hydroxyapatite obtained by the gelcasting of foams, J. Am. Ceram. Soc. 83 (2000) 3021–3024.